HGT

Open camera or QR reader and scan code to access this article and other resources online.

# A Modified Arrestin1 Increases Lactate Production in the Retina and Slows Retinal Degeneration

Tiffany S. Nelson, Chiab Simpson, Frank Dyka, Astra Dinculescu, and W. Clay Smith*

*Department of Ophthalmology, University of Florida, Gainesville, Florida, USA.*

Glucose metabolism in the retina is carefully orchestrated, with glucose being delivered to photoreceptors from the choroidal circulation through the retinal pigmented epithelium (RPE). In photoreceptors, glucose is processed principally by aerobic glycolysis, from which the lactate byproduct is provided to the RPE and Müller glia for their energetic needs. In this study, we utilize a modified arrestin1 protein to enhance the glycolytic output of lactate from rod photoreceptors through disinhibition of enolase1 activity with the goal being to use this increased lactate production as a gene-agnostic approach to slowing retinal degeneration. Mouse arrestin1 with E362G/D363G amino acid substitutions (referred to as ''ArrGG'') was packaged into AAV and tested for safety and for efficacy in increasing retinal lactate production. Overexpression of ArrGG in C57BL/6J mice did not result in any detectable changes in either electroretinogram (ERG) function or photoreceptor survival as measured by outer nuclear layer (ONL) thickness. However, mouse retinas expressing ArrGG showed a $\sim$25% increase in the rate of lactate secretion.

Therefore, AAV-ArrGG was delivered intravitreally to heterozygous P23H rhodopsin knockin mice ($Rho^{P23H/+}$) to determine if enhancing glycolysis in photoreceptors can slow retinal degeneration in this animal model of retinitis pigmentosa. We found that the expression of ArrGG in these mice slowed the decline of both scotopic and photopic ERG function. Correspondingly, there was significant preservation of ONL thickness in $Rho^{P23H/+}$ mice treated with ArrGG compared with controls. In conclusion, our studies show that expressing ArrGG in C57BL/6J mouse retina results in an increase in lactate production, consistent with an upregulation of glycolysis. In the P23H rhodopsin model of retinitis pigmentosa, the expression of ArrGG led to significant preservation of photoreceptor function and slowing of retinal degeneration. These findings suggest that enhancing glycolysis by targeting increased enolase1 activity with a modified arrestin1 in photoreceptors may offer a therapeutic approach to slowing retinal degeneration.

**Keywords:** gene therapy, metabolism, glycolysis, photoreceptors, enolase

## INTRODUCTION

INHERITED RETINAL DISEASES (IRDs) are a world-wide health problem, affecting more than two million people.[1–3] IRDs are genotypically and phenotypically diverse, with more than 270 genes identified to date that cause retinal degeneration, many of which have multiple causative mutations within each gene (RetNet, https://sph.uth.edu/RetNet/).[4] This genetic and phenotypic diversity presents a challenge for treating IRDs with traditional gene therapy approaches that target the specific underlying genetic defect, such as the use of voretigene neparvovec (Luxturna™) to target the RPE65 defect in Leber's congenital amaurosis-2.[5,6] This treatment for an IRD, while groundbreaking, is limited by the genetic diversity of IRDs and the cost of developing precision genetic therapies.[7]

This limitation of gene-specific strategies has provided the impetus for a variety of approaches that seek to slow

*Correspondence: Prof. W. Clay Smith, Department of Ophthalmology, University of Florida, Gainesville, FL 32610-0284, USA. E-mail: wcsmith@ufl.edu

or halt the progression of vision loss without specifically targeting the genetic defect, such as electronic retinal implants,[8,9] optogenetic approaches to provide light sensitivity to second- and third-order retinal neurons,[10] and transplant therapies using induced pluripotent stem cells.[11]

Another approach to slowing vision loss capitalizes on the fact that the neural retina is one of the most energetically demanding tissues in the body.[12] The therapeutic idea is that enhancing metabolism in this highly active tissue will make the retina resistant to the underlying genetic insult, slowing the progression of vision loss, which may not become evident until the later decades of life in many IRDs. These metabolism-targeting approaches include the use of neurotrophic factors,[13] targeting mitochondrial biogenesis,[14] enhancing photoreceptor use of lactate,[15,16] and upregulation of glycolytic enzyme expression.[17,18]

Targeting photoreceptors as a mechanism to selectively improve metabolism has a unique appeal from both a consumer and producer perspective. First, photoreceptors are enormous energy consumers, using on the order of $10^5$ $ATP \cdot s^{-1}$ for each rod and cone,[19] making them one of the most metabolically active cells in the entire body.[20,21] Surprisingly, this metabolic demand is met largely through aerobic glycolysis of glucose, despite the relatively low energy output from glycolysis compared with oxidative phosphorylation. However, it is this use of glycolysis that also makes photoreceptors important producers for the retina since the lactate byproduct of glycolysis is secreted by the photoreceptors to the surrounding Müller glia and retinal pigmented epithelium (RPE) for use by these cells as their primary energy supply.[21]

In this study, our goal was to take advantage of the central role that photoreceptors play in the metabolic health of the retina and specifically enhance their glycolytic output by modulating enolase1 activity, one of the central enzymes in glycolysis. To accomplish this goal, we turned to a previous observation we made in which we noted that the enzymatic activity of enolase1 was diminished by an interaction with arrestin1.[22] Our recent study showed the mechanism of this effect, demonstrating that two amino acids of arrestin1 are largely responsible for sterically inhibiting access of 2-phosphoglycerate (2-PGA) substrate to enolase1.[23] Importantly, we showed that substituting the relatively large side chains of Glu-361 and Asp-362 with glycine residues completely removed the inhibitory effect of bovine arrestin1 on enolase1 catalysis.

Our hypothesis in this study is that we could potentially increase the glycolytic rate in photoreceptors by using an arrestin1 that was modified to include these two glycine residues to competitively disinhibit the effect of arrestin1 on enolase1. Increasing glycolysis will provide more ATP to photoreceptors and additional metabolic support to the surrounding cells in the form of secreted lactate. Consequently, this approach is expected to make the retina more resistant to damage, such as that caused by inherited genetic defects, and slow retinal degeneration without targeting the specific defect.

## METHODS

### Animals

This study was conducted under the approval of the University of Florida's Institutional Animal Care and Use Committee and in accordance with the Association for Research in Vision an Ophthalmology's statement for the Use of Animals in Ophthalmic and Vision Research.

### Strains

Arrestin1 knockout mice ($Sag^{tm1Jnc}$)[24] and rhodopsin P23H knockin mice ($Rho^{P23H/P23H}$)[25] were obtained from Jackson Laboratories (Bar Harbor, ME) and maintained as in-house breeding colonies with genotypes confirmed by PCR.[25] $P23H^{+/-}$ (*i.e.,* $Rho^{P23H/WT}$) were obtained by breeding with C57BL/6J wild-type mice and tested for the lack of *Rd1* and *Rd8* mutations. The arrestin1 knockout mice used in experiments were reared in dim red lighting to avoid retinal degeneration that can be caused by exposure to bright light.[24] Mice heterozygous for both P23H and for arrestin1 (*i.e.,* $Rho^{P23H/WT}\,Arr1^{WT/-}$) were obtained by breeding $Rho^{P23H/P23H}$ with $Arr1^{-/-}$ mice.

### Lactate secretion assays

Retinal lactate secretion was measured using retinas obtained from mice that were dark adapted overnight. Under dim red light, mice were euthanized by isoflurane overdose followed by cervical dislocation. The retina was isolated from the eye through a slit in the cornea and separated from the RPE and lens. The retina was placed in Dulbecco's modified Eagle's medium (DMEM) prewarmed to 37°C and maintained on a 37°C heating block. The DMEM contained 4.5 g/L glucose and no additional glycolytic fuels. Aliquots of the media were removed at 1-min intervals. All procedures to this point were conducted under dim red lighting.

The concentration of lactate in the collected media samples was determined in triplicate using the Lactate-Glo Luciferase Assay (Promega #J5021). The rate of lactate secretion was derived by linear regression analysis of the determined lactate concentrations collected over the time interval, comparing lactate rates between groups by one-way analysis of variance (ANOVA) with Tukey's *post hoc* comparison (GraphPad Prism, v9.2.0).

### Glucose uptake assays

Retinal glucose uptake was measured similar to the lactate secretion assay above, except that the dark-adapted retinas were placed in DMEM containing only 1 mM glucose. Glucose levels were collected at 1-min intervals under dim red lighting. Glucose concentrations were determined using the Glucose-Glo luciferase assay (Promega

#J6021). The rate of glucose uptake was derived by linear regression analysis of the determined glucose concentrations collected over the time interval, comparing glucose rates between groups by parametric unpaired *t*-test, (GraphPad Prism, v9.2.0).

### Arrestin1-enolase1 retinal concentration

To determine the concentration of arrestin1 in the mouse retina relative to enolase1, retinal extracts were prepared from C57BL/6J mice using three retinas from three different mice. Isolated retinas were placed in Laemmli's sample buffer[26] and sonicated to disrupt the tissue. A two-fold serial dilution of each extract was electrophoresed in duplicate on 12% SDS-polyacrylamide gels and transferred to polyvinylidene fluoride membrane, loading a serial dilution of known arrestin1 quantities on one gel, and a serial dilution of enolase1 quantities on the other. Purified murine arrestin1 and murine enolase1 were obtained by heterologous expression and purification of His(6)-tagged proteins in *Pichia pastoris* as previously described.[22]

Quantitation of the protein standards, purified to >95% homogeneity, was determined spectrophotometrically, using extinction coefficients for arrestin1 (22,330 $M^{-1}$) and enolase1 (32,430 $M^{-1}$). Blots were probed with 1 $\mu$g/mL C10C10 monoclonal anti-arrestin1 antibody,[27] and 1 $\mu$g/mL Enol2–53 monoclonal antibody, which is specific for the enolase1 isoform.[22] Antibody binding was detected with anti-mouse conjugated to infrared fluorophore IRDye 680RD (Li-Cor #926-68070) then imaged and quantified with an Odyssey CLX (Li-Cor).

### Lactate dehydrogenase concentrations

Relative levels of lactate dehydrogenase A (LDHA) were assessed in retinas used in the lactate secretion assays by immunoblotting. For these samples, retinas were recovered from the media after the final time point was collected, and homogenized in 250 $\mu$L phosphate-buffered saline with 0.1% dodecyltrimethylammonium bromide. After centrifugation (5 min; 18,000 *g*), the soluble sample was removed.

Protein concentrations of the retinal extracts were determined by BCA assay (Thermo Fisher #23235). Since the protein content of all retinal extracts were within 10% of each other, 10 $\mu$L of each retinal extract was used without further adjustment. All samples were mixed with Laemmli's sample buffer and immunoblotted as described above. Duplicate blots were probed with either anti-LDHA (1:1,000; Cell Signaling Technology #2102) or anti-$\beta$-tubulin (1 $\mu$g/mL Santa Cruz #SC-5274).

### Construction of AAV vectors

Murine arrestin1 (ArrWT) cDNA was obtained by polymerase chain reaction amplification from reverse-transcribed poly(A)-RNA isolated from C57BL/6J mouse retinas (the QuickPrep Micro mRNA Kit#27-9255-01 and First-Strand cDNA synthesis Kit#27-9261-01; GE Healthcare) using primers specific for the murine arrestin1 open-reading frame, and incorporating a myc-tag immediately before the stop codon. PCR products were cloned into the *Eco*RI and *Not*I sites of pDsRed2-N1 by Gibson assembly (the NEBuilder Gibson Assembly Cloning Kit; New England Biolabs #E5510).[28] This ArrWT plasmid was then used to introduce the E362G/D363G double glycine mutations (ArrGG) into the same backbone with the QuikChange II Site-Directed Mutagenesis Kit (Agilent, #200521).

The ArrWT and ArrGG cDNAs were transferred to the *Not*I site of pTR-hOp181opt, placing the arrestin1 cDNA under the control of a 181 bp human opsin promoter with optimized *Crx*-binding sites. In this promoter, the first and third *Crx*-binding sites were changed from CAATTAGG and GAGCTTAG to CTAAGCCC and CTAATCCC, respectively, driving high-level expression of the transgene selectively in rod photoreceptors.[29]

These pTR-hOp181opt-ArrWT-myc and pTR-hOp181opt-ArrGG-myc plasmids were used to generate AAV vectors using a triple-plasmid transfection method in human embryonic kidney cells (HEK-293T). In each case, the transgene was packaged into an AAV2-based vector containing four tyrosine-to-phenylalanine (Y272, 444, 500, 730F) plus one threonine-to-valine substitution (T491V) in the capsid, which has been shown to have excellent penetration of the murine retina and transduction of photoreceptors when delivered intravitreally.[30,31] AAV vectors were packaged, purified, endotoxin cleaned, and titered by the Ocular Gene Therapy Core at the University of Florida as previously described.[32]

### *In vitro* competitive disinhibition of enolase1

Enolase1 catalytic activity was measured *in vitro* using a reconstitution assay as previously described.[23] Briefly, the increase in absorbance at 240 nm from the catalytic processing of 2-PGA to phosphoenolpyruvate was monitored as a measure of enolase1 catalytic activity. In this assay, 1 mM 2-PGA was mixed with 50 nM murine enolase1 with and without 100 nM murine arrestin1 (ArrWT). To this mixture, increasing amounts of ArrGG (0–200 nM) was added and the enzymatic turnover number calculated using an extinction coefficient of 1,520 $M^{-1}$ for phosphoenolpyruvate. Rates of turnover were derived by linear regression analysis (GraphPad Prism, v9.2.0).

### Intravitreal injections

Before injections and immediately before applying anesthetic, each mouse had their eyes dilated with 0.25% phenylephrine HCL and 1% tropicamide applied topically to the eye. A single intraperitoneal injection of xylazine (5–10 mg/kg) and ketamine (70–100 mg/kg) in sterile saline solution was given for anesthesia. Using a 33 G needle, a small scleral puncture, 2 mm from limbus, was made under an operating microscope, followed by injection

of 1.0 $\mu$L of virus ($3.0\times10^9$ vg/$\mu$L) or 1 $\mu$L of buffer delivered to the intravitreal space in one eye and the contralateral eye, respectively. Application of 0.3% GenTeal gel (Novartis) to the corneal surface aided in visualizing needle insertion into the vitreous cavity without penetrating the lens or the retina.

Upon recovery from anesthesia, the mice were returned to the vivarium where they were maintained on a 12-h light–12-h dark cycle.

### Electroretinographic analysis

Electroretinograms (ERG) were recorded at approximately monthly intervals postinjection using the Celeris™ ERG system (Diagnosis LLC). All ERGs were recorded using Espion V6.0.52 software. Mice were dark adapted overnight, providing food and water *ad libitum*. Before recording, mice eyes were dilated and anesthetized as described above. Anesthetized mice were maintained at 37°C throughout the ERG. The electrodes were placed in gentle contact with both eyes, with reference electrodes placed subcutaneously into the head and tail. Scotopic ERGs were recorded at 0.01, 1.0, and 3.0 $cd\cdot s\cdot m^{-2}$. Each intensity included five light flashes with 20 s between each flash. Following a 2-min light adaptation at 30 $cd\cdot s\cdot m^{-2}$, photopic ERGs were recorded at 2.0, 10.0, and 30.0 $cd\cdot s\cdot m^{-2}$ with 25 flickers at each intensity.

The amplitude of the a-wave was calculated as the peak of decrease of the waveform within 15 ms of the flash, and b-wave amplitude was calculated as the potential between the a-wave minimum and b-wave maximum within 100 ms of the flash. Amplitudes of a-waves and b-waves under scotopic and photopic conditions were compared by parametric paired *t*-test, comparing the AAV-treated eye with the contralateral buffer eye (GraphPad Prism, v9.2.0).

### Optical coherence tomography

At approximately monthly intervals postinjection, optical coherence tomography (OCT) was performed to analyze retinal structure. OCT was performed using the HRA+OCT Spectralis (Heidelberg Engineering), dilating and anesthetizing as described above. The outer nuclear layer (ONL) thickness was measured at 300 $\mu$m intervals from the optic nerve in the temporal–nasal plane using the Heidelberg software with calibrated calipers. ONL thickness between groups was compared by one-way ANOVA with Tukey's *post hoc* comparison (GraphPad Prism, v9.2.0).

### Immunohistochemistry and microscopy

Whole mouse eyes were dissected from the orbit and placed in buffered 4% paraformaldehyde for 1 h. The sclera was then punctured with a tuberculin needle and returned to the fixative overnight at 4°C. Eyes were embedded in paraffin and sectioned. Deparaffinized slides were stained for arrestin1 with 10 $\mu$g/mL C10C10 mouse monoclonal antibody,[27] and for myc-antigen with 1:250 71D10 rabbit monoclonal antibody (Cell Signaling #2278). Antibody binding was detected with 8 $\mu$g/mL anti-mouse-AlexaFluor488 (Invitrogen #A11029) and 8 $\mu$g/mL anti-rabbit-AlexaFluor594 (Invitrogen #A11037) with 10 $\mu$g/mL DAPI (Invitrogen #D1306) used for nuclear staining. Sections were imaged with a Leica SP8 confocal microscope, collecting Z-stack images at 0.5 $\mu$m intervals and then creating a maximum projection of the Z-stack.

## RESULTS

### Expression of ArrGG in wild-type mice

Enhancing glycolysis in photoreceptors has the potential to broadly improve the overall metabolic health of the retina. Our hypothesis is that introducing a modified arrestin1 that disinhibits enolase1 catalysis should increase glycolytic output by competing with endogenous arrestin1. To determine if this hypothesis has any basis, we first examined the rate of lactate production in mice expressing reduced amounts of arrestin1. Our logic was that if arrestin1 is functionally suppressing glycolytic output, then this effect should be revealed by reducing expression of endogenous arrestin1.

For this experiment, we took advantage of the arrestin1 knockout mouse ($Sag^{tm1Jnc}$)[24], which expresses $\sim$50% of the arrestin1 content in heterozygous animals ($Arr1^{+/-}$). Retinas of dark-adapted mice were excised and placed in DMEM culture media and the time course of lactate secretion into the media was determined as a measure of glycolytic output (Fig. 1A, B). Mice with reduced levels of arrestin1 showed a significant increase in the rate of lactate secretion, with lactate production rates increased by 21% in $Arr1^{+/-}$ and 38% in $Arr1^{-/-}$ mice compared with their wild-type littermates ($Arr1^{+/+}$).

This increase in lactate secretion from the retina is consistent with the concept that decreasing the expression level of arrestin1 reduces the inhibition of arrestin1 on enolase1. To further test this idea, we also examined the rate of glucose uptake from the media by $Arr1^{+/-}$ and $Arr1^{+/+}$ retinas (Fig. 1C). Consistent with the lactate production results, there was enhanced consumption of glucose by the $Arr1^{+/-}$ mice compared with $Arr1^{+/+}$ mice.

One alternative explanation for the difference in lactate secretion and glucose uptake is that lactate dehydrogenase levels are different between the genotypes. To assess this idea, we prepared extracts from the retinas used in the lactate secretion assays and performed immunoblotting for LDHA, the most abundant LDH isoenzyme found in photoreceptors.[33,34] Across all three genotypes, there was no evidence of change in LDHA expression levels (Fig. 1D).

A second consideration before advancing with the idea of arrestin1 disinhibition of enolase1 to increase glycolytic output in photoreceptors is to consider the relative molar ratio of arrestin1 and enolase1. If the concentration of

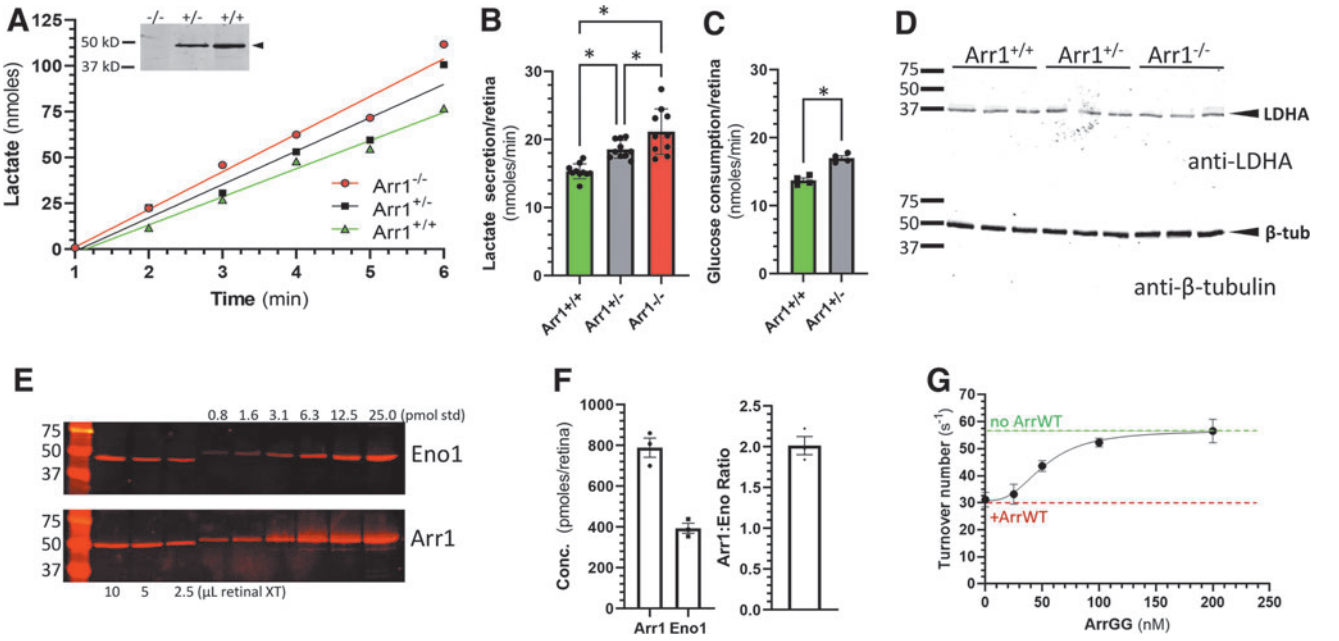


**Figure 1.** Rate of lactate production in retinas from mice expressing reduced levels of arrestin1. **(A)** Example of time course of lactate secretion from excised, dark-adapted retinas placed in DMEM from *Arr1*$^{+/+}$, *Arr1*$^{+/-}$, and *Arr1*$^{-/-}$ mice; *inset* shows anti-arrestin1 immunoblot of retinal extracts from the three *Arr1* genotypes, demonstrating that arrestin1 expression in *Arr1*$^{+/-}$ is ~50% of wild-type levels, and is not detectable in *Arr1*$^{-/-}$ (extracts of retinas from the indicated genotype were probed with C10C10 anti-arrestin1 antibody). **(B)** Average rates of lactate secretion derived from retinas from **(A)**; mean ± SD ($n$ = 10 retinas, 5 mice). **(C)** Average rates of glucose consumption of retinas from *Arr1*$^{+/+}$ and *Arr1*$^{+/-}$ mice; mean ± SEM ($n$ = 4 retinas). **(D)** Lactate dehydrogenase levels in different *Arr1* genotypes are unchanged; extracts from three retinas used in **(B)** for each *Arr1* genotype (*Arr1*$^{+/+}$, *Arr1*$^{+/-}$, and *Arr1*$^{-/-}$) were immunoblotted and probed with anti-LDHA (upper blot) or anti-$\beta$-tubulin (lower blot). **(E)** Quantitation of arrestin1 and enolase1 expression in whole retinal extracts of C57BL/6J mice. An example of enolase1 immunoblotting (Eno1) and arrestin1 immunoblotting (Arr1) are shown comparing three different volumes (in $\mu$L) of retinal extract with known quantities of purified enolase1 and arrestin1 (in pmoles). **(F)** Quantitation of multiple blots as in **(E)**, showing the average concentration of arrestin1 and enolase1 and molar ratios in each retina (bars show mean ± SEM; $n$ = 3 retinas). **(G)** Inhibition of enolase1 catalysis by arrestin1 (ArrWT) is competitively reduced by addition of ArrGG; the rate of turnover of 2-PGA was monitored in the presence of 50 nM enolase1 without ArrWT (*green dashed line*) or with 100 nM ArrWT (*red dashed line*). Addition of the indicated concentration of ArrGG reduced the suppression of enolase1 catalysis caused by ArrWT (points show mean ± SEM; $n$ = 3). 2-PGA, 2-phosphoglycerate; DMEM, Dulbecco's modified Eagle's medium; LDHA, lactate dehydrogenase A; SD, standard deviation; SEM, standard error of the mean. Color images are available online.

arrestin1 greatly exceeds that of enolase1, then a strategy to compete for arrestin1 binding to enolase1 with a modified arrestin1 is likely to be ineffectual.

Therefore, we performed quantitative western blot analysis to determine the molar concentration of arrestin1 relative to enolase1 in whole mouse retina, comparing the endogenous levels of arrestin1 and enolase1 to a series of known arrestin1 and enolase1 quantities (Fig. 1E). From this analysis, the amount of arrestin1 and enolase1 in a whole mouse retina was determined to be 788 pmoles/retina (±47.2, $n$ = 3) and 393 pmoles/retina (±24.5, $n$ = 3), respectively, in adult C57BL/6J mice, with a molar ratio of 2:1 arrestin1 to enolase1 (Fig. 1F).

This value for arrestin1 concentration in retinas is in good agreement with the 584 pmoles/retina value determined in previous quantitative studies,[35] assuming there are ~6.4 million rods per retina.[36] Thus, the concentration of arrestin1 is well within an order of magnitude of enolase1 (Fig. 1F), suggesting that overexpression of a modified arrestin1 could be an effective competitor for native arrestin1.

We have previously shown that arrestin1 binds enolase1 along the surface that is opposite the side where arrestin1 binds photoactivated rhodopsin.[23] In this interaction, two charged residues of arrestin1 (Glu-361 and Asp-362 in bovine arrestin1) sterically interfere with one of the catalytic centers of the enolase1 dimer. In tissue culture, changing these amino acids to glycine completely removes the inhibitory effect of arrestin1.[23]

Before advancing to *in vivo* studies, we assessed whether the modified arrestin1 could be used to competitively disinhibit the effect of wild-type arrestin1 on enolase1 catalysis. To make this assessment, homologous substitutions were made in murine arrestin1 (*i.e.,* E362G/D363G; hereafter referred to as ArrGG for the two glycine substitutions) and heterologously expressed for an enolase activity assay. In this assay, the rate of 2-PGA catalysis to PEP by murine enolase1 was monitored with and without inhibition by wild-type murine arrestin1 (ArrWT). As expected, addition of ArrWT causes a decrease in enolase1 catalytic rate (Fig. 1G). The inclusion of increasing concentrations of ArrGG results in increasing enolase1 activity, indicating effective competitive disinhibition of ArrWT on enolase catalysis by ArrGG.

To determine if this *in vitro* observation of competitive disinhibition could be translated *in vivo* in the murine retina, the ArrGG was packaged in AAV to deliver the modified arrestin1 to the mouse retina. For this AAV

vector, ArrGG was cloned into the pTR-AAV backbone behind a modified opsin promoter (Fig. 2A), introducing a C-terminal myc-tag (EQKLISEEDL) to allow for detection of the AAV-delivered arrestin1. This modified arrestin1 was then packaged into AAV2-quadY-F +T-V[31] and injected intravitreally into C57BL/6J mice in one eye, with the contralateral eye receiving an intravitreal injection of the saline excipient.

Mice receiving ArrGG were evaluated for ERG function 60 days postinjection. The individual wave form kinetics and scotopic intensity response function were indistinguishable in mice injected with ArrGG compared with mice receiving buffer injections for both the a-wave and b-wave responses (Fig. 2B).

A similar lack of effect was seen for the light-adapted photopic b-wave responses. In OCT, mice injected with

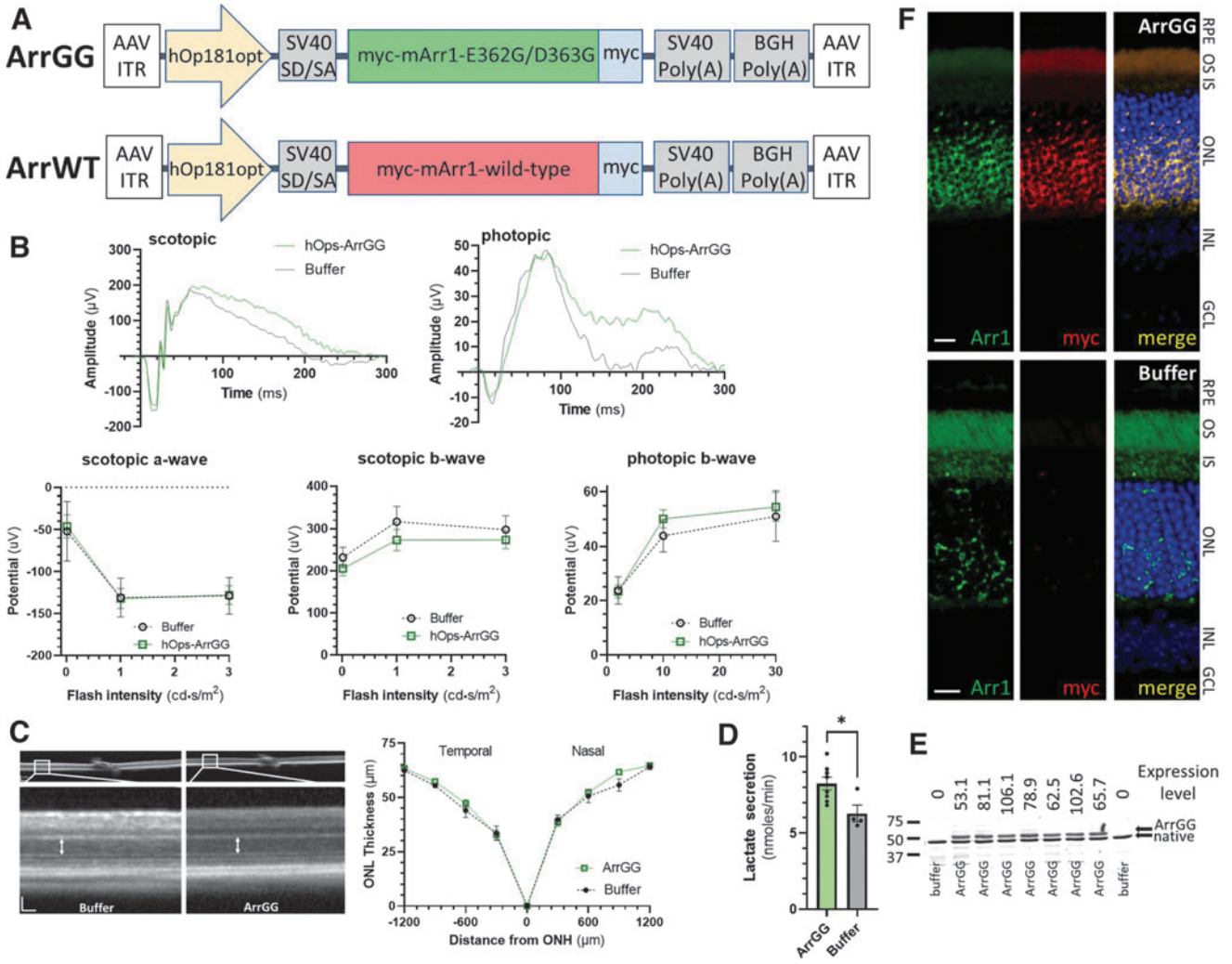


**Figure 2.** Safety and efficacy of ArrGG overexpression in adult C57BL/6J mouse retina. **(A)** Design of AAV vectors with myc-tagged modified arrestin1 (ArrGG) and wild-type arrestin1 (ArrWT) transgene expression driven by a human rod-specific opsin promoter (hOp181opt). The expression cassette is flanked by ITR of AAV serotype 2. **(B)** ERG responses at 60 days postinjection; example raw scotopic and photopic responses from an animal injected with ArrGG (*green*) compared with one injected with buffer (*gray*) are shown above; flash intensity response curves for scotopic and photopic amplitudes were not significantly different in eyes injected with ArrGG ($n=8$) compared with eyes injected with just buffer ($n=4$); points represent mean ± SEM. **(C)** Example of ONL thickness measured by OCT in mouse injected with buffer (*left* image) or ArrGG (*right* image; scale bars, 50 $\mu$m); spider gram plot of ONL thickness measured in eyes treated with ArrGG (*green curves*; $n=8$) shows no significant different compared with eyes receiving buffer only (*black curves*; $n=4$); points represent mean ± SEM. **(D)** Lactate secretion rates in retinal explants from mice treated with ArrGG (*green*; $n=8$) and mice receiving buffer only (*gray*; $n=4$); bars show mean ± SEM, *asterisk* indicates statistically significant difference in parametric paired *t*-test ($\rho < 0.05$). **(E)** Immunoblot quantitation of ArrGG expression relative to endogenous arrestin1; blots of soluble extracts of retinas used in **(D)** from seven eyes injected with AAV-ArrGG and two eyes injected with buffer (indicated below blot) were probed with anti-arrestin1 antibody, which identifies the higher molecular mass ArrGG (with a myc-tag) and the native arrestin1; values above each lane indicate the amount of ArrGG expressed as a percentage of the native arrestin1. **(F)** Immunohistochemistry of representative mouse retinal sections; paraffin sections of eyes injected with AAV-ArrGG or buffer were stained for arrestin1 (*green*) or for myc antigen (*red*), and nuclei stained with DAPI (*blue*). Scale bars, 10 $\mu$m. ERG, electroretinograms; GCL, ganglion cell layer; INL, inner nuclear layer; IS/OS, inner segment/outer segment layers; OCT, optical coherence tomography; ONL, outer nuclear layer; RPE, retinal pigmented epithelium. Color images are available online.

ArrGG showed no indications of inflammatory response, with good stratification of retinal layers (Fig. 2C). Measurement of ONL thickness as a proxy for photoreceptor survival in these OCT images showed no statistically significant difference in mice expressing ArrGG compared with eyes injected with buffer (Fig. 2C).

Following OCT and ERG measurements, the retinas were extracted and the rate of glycolysis was assessed by measuring the rate of lactate secretion from retinas placed *ex vivo* in DMEM containing excess glucose as described above. In these retinas, the mice that received ArrGG showed a significantly increased rate of lactate production compared with retinas from buffer-injected mice (ArrGG: $8.3 \pm 0.42$ nmoles$\cdot$min$^{-1}$; Buffer: $6.3 \pm 0.55$ nmoles$\cdot$min$^{-1}$; $\rho = 0.020$) (Fig. 2D).

We also performed immunoblotting of extracts from these retinas to determine the levels of transgene expression. Samples of the same retinas used in Fig. 2D show that the myc-tagged ArrGG is expressed on average at 78% of endogenous arrestin1 levels (range 53–106%) (Fig. 2E). Injected eyes were also examined by immunohistochemistry for localization of ArrGG expression.

Staining of sections from eyes injected with the myc-tagged ArrGG showed that expression of the ArrGG transgene is detected in the photoreceptor layers (ONL, inner segments, and outer segments), coinciding with the localization of arrestin1 (Fig. 2F). These representative images reflect the largely uniform expression of the ArrGG transgene that is achieved with intravitreal delivery of the AAV. As expected, myc-reactivity is not detected in buffer-injected controls. These sections reveal a healthy appearance of the retina, with well-organized retinal layers.

These findings show that overexpression of ArrGG did not have a measurable impact on either ERG function or photoreceptor cell survival as monitored by ONL thickness and histological sectioning. However, retinas from eyes that received ArrGG showed a 22% higher rate of lactate production, consistent with an increased rate of glycolytic activity.

### Expression of ArrGG in Rho-P23H mice

Our results prompted us to further examine whether this targeted improvement in lactate production could potentially be used therapeutically to slow photoreceptor loss in a model of retinal degeneration. For this experiment, we selected the P23H heterozygous knockin mouse model ($Rho^{P23H/+}$, Jackson Stock No: 017628).[25] This mouse expresses one copy of the P23H mutation in the rhodopsin gene and shows a moderate rate of retinal degeneration, losing nearly all photoreceptors by P120[25,37–41] (for ease of notation, we hereafter refer to this heterozygous mouse line as $P23H^{+/-}$).

In our study, $P23H^{+/-}$ mice were injected at P30, before significant loss of photoreceptors is evident,[25] and then followed out to P130, at which point the photoreceptor loss is significantly advanced. Mice were injected intravitreally in one eye with either ArrGG or ArrWT, with the contralateral eye receiving an equivalent injection of buffered saline solution.

OCT assessment of ONL thickness at approximately monthly intervals showed a rapid thinning of the ONL in $P23H^{+/-}$ eyes that received buffer (Fig. 3A, black curve), consistent with previous reports.[25] Similarly, mice injected with ArrWT showed a comparable decline in ONL thickness (Fig. 3A, red curve). In contrast, eyes that were injected with ArrGG showed significantly thicker ONL (Fig. 3A, green curve). This difference was noted as early as 30 days postinjection and persisted out to P130 when the mice were sacrificed. Note that the typical ONL thickness in a nondegenerating retina is $\sim 60\ \mu$m.

Paraffin sections of these $P23H^{+/-}$ eyes were stained and showed comparable results. Mice that were injected with ArrGG showed significantly more rows of ONL nuclei (6–7 rows; Fig. 3B) than $P23H^{+/-}$ eyes that were injected with either wild-type arrestin1 (Fig. 3C) or buffer (Fig. 3D). In these latter two groups, only 2–3 rows of nuclei were present at P130. The photoreceptor inner/outer segment layer was also thicker in the ArrGG-injected eyes compared with either the ArrWT- or buffer-treated animals.

To assess whether the slowed ONL thinning observed in OCT imaging was reflected in preservation of photoreceptor electrical response, the treated mice were also assessed for ERG function. Example traces from an ArrGG-treated $P23H^{+/-}$ mouse show that at each intensity of light, the eye injected with ArrGG showed a higher response amplitude than the contralateral untreated eye (Fig. 4A). In contrast, an example $P23H^{+/-}$ mouse receiving injections of ArrWT showed no increase in response amplitude compared with the buffer-treated contralateral eye (Fig. 4C).

These observations in individual animals were recapitulated across the cohort, in which animals treated with ArrGG show a statistically significant preservation of both a-wave and b-wave amplitudes compared with the buffer-injected control eyes (Fig. 4B). This preservation of ERG function is absent in mice that were injected with ArrWT (Fig. 4D).

Although our AAV vector is targeted for selective expression of the transgene in rod photoreceptors through the human rod opsin promoter, there is the possibility of achieving a bystander effect in cones. To assess whether cone function was preserved, we also measured ERGs under photopic conditions. The results show a significant preservation of the photopic b-wave function in eyes that were injected with ArrGG compared with buffer-injected control eyes (Fig. 4E). In contrast, delivery of ArrWT provided no preservation of ERG function.

We also measured the rate of lactate secretion from $P23H^{+/-}$ retinas to assess glycolytic potential in eyes treated with ArrGG compared with either injection with wild-type arrestin1 or buffer (Fig. 5). These results showed

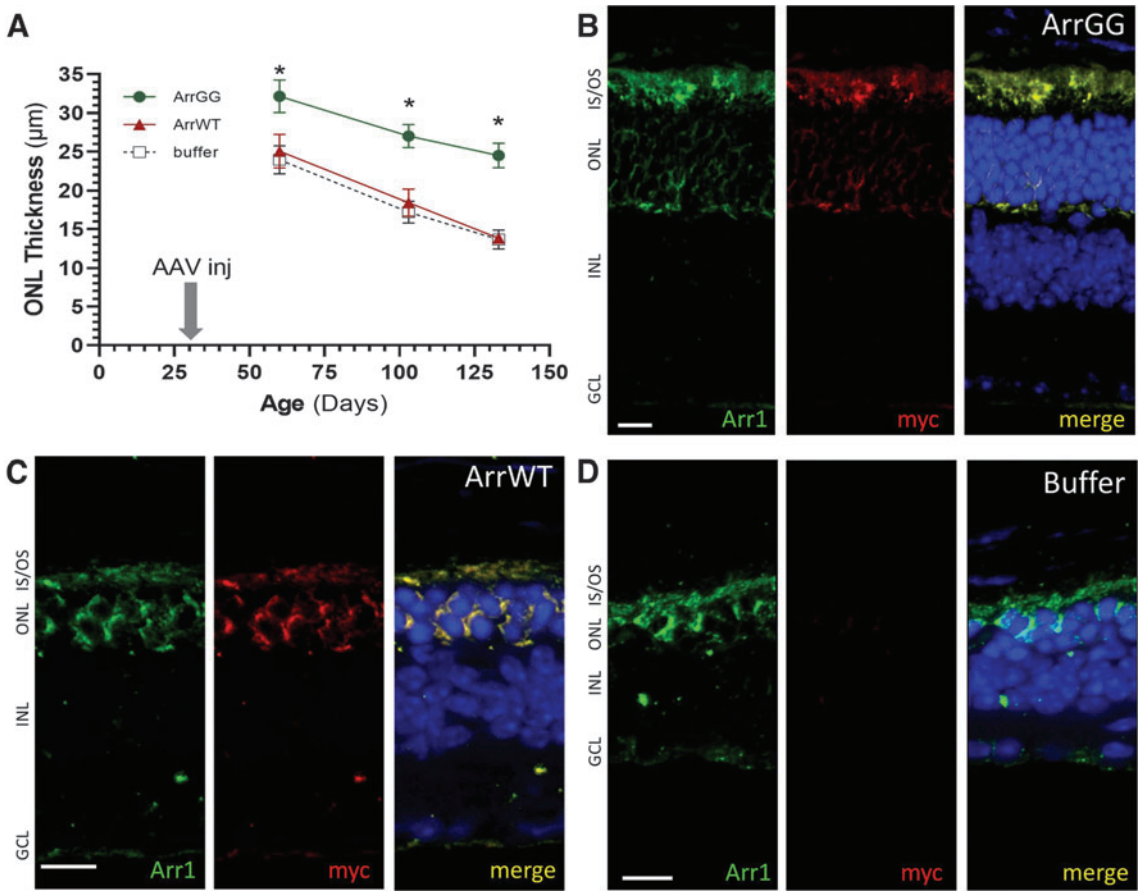


**Figure 3.** Photoreceptors are preserved in *P23H*$^{+/-}$ mice treated with ArrGG. **(A)** ONL thickness was measured in *P23H*$^{+/-}$ mice from OCT images collected at approximately monthly intervals following injection of *P23H*$^{+/-}$ mice at PN30 with either AAV-ArrGG (*green curves*), AAV-ArrWT (*red curves*), or buffer only (*black curves*); ONL measurements are shown at 1,200 $\mu$m from the optic nerve head in the temporal retina (ONL thickness is typically 60 $\mu$m in nondegenerating retinas). Statistical comparison at each time point showed significantly thicker ONL in eyes treated with ArrGG, compared with eyes treated with either ArrWT or buffer (one-way ANOVA; *asterisk* indicates $\rho < 0.05$); points show mean ± SEM. **(B)** Example paraffin section of *P23H*$^{+/-}$ mouse retina injected with ArrGG at P30 and collected at P130. **(C)** Example paraffin section of *P23H*$^{+/-}$ mouse retina injected with ArrWT at P30 and collected at P130. **(D)** Example paraffin section of *P23H*$^{+/-}$ mouse retina injected with buffer at P30 and collected at P130. Sections stained with anti-arrestin1 (*green*), anti-myc (*red*), and DAPI (*blue*). Scale bars, 10 $\mu$m. ANOVA, analysis of variance. Color images are available online.

a nearly threefold improvement in lactate secretion rates in the eyes that were treated with ArrGG compared with eyes that received either ArrWT or buffer sham injections. This rate of lactate secretion is significantly higher than the 25% increase that would be achieved by complete disinhibition of enolase1 and likely reflects the significant preservation of photoreceptors that is seen in the ArrGG-treated eyes.

Finally, these observations of preserved photoreceptor function in *P23H*$^{+/-}$ mice suggest that if our approach of overexpression of ArrGG is functioning through enhanced lactate production, then a similar protective effect should be seen by reducing arrestin1 expression such as was seen in the *Arr1*$^{+/-}$ mice with 50% expression of arrestin1 (Fig. 1). To test this idea, *P23H*$^{-/-}$ mice were crossed with *Arr1*$^{-/-}$ to generate mice that were heterozygous at both genes (*i.e.*, *P23H*$^{+/-}$ *Arr1*$^{+/-}$).

These mice were examined by ERG and OCT at ~3 months of age when photoreceptor loss is clearly evident in *P23H*$^{+/-}$ and compared with mice that express the normal amount of arrestin1 (*i.e.*, *P23H*$^{+/-}$ *Arr1*$^{+/+}$). Scotopic a-wave and b-wave ERG function in the *P23H*$^{+/-}$ mice was significantly better when the *P23H*$^{+/-}$ mice were on the *Arr1*$^{+/-}$ background than on the *Arr1*$^{+/+}$ background (Fig. 6A). This improvement in photoreceptor electrical function was also reflected in a significant preservation of photoreceptor ONL thickness when assessed by OCT for *P23H*$^{+/-}$ mice on the *Arr1*$^{+/-}$ background (Fig. 6B).

## DISCUSSION

Our previous studies of the arrestin1/enolase1 interaction identified an inhibition of enolase1 activity by ~25% under *in vitro* reconstitution conditions,[22] and was confirmed in tissue culture with HEK-293T cells.[23] This current study extends these findings to the retinal photoreceptors, where arrestin1 and enolase1 colocalize. Our *in vivo* study indicates that arrestin1 expression similarly partially suppresses the production of lactate in the retina.

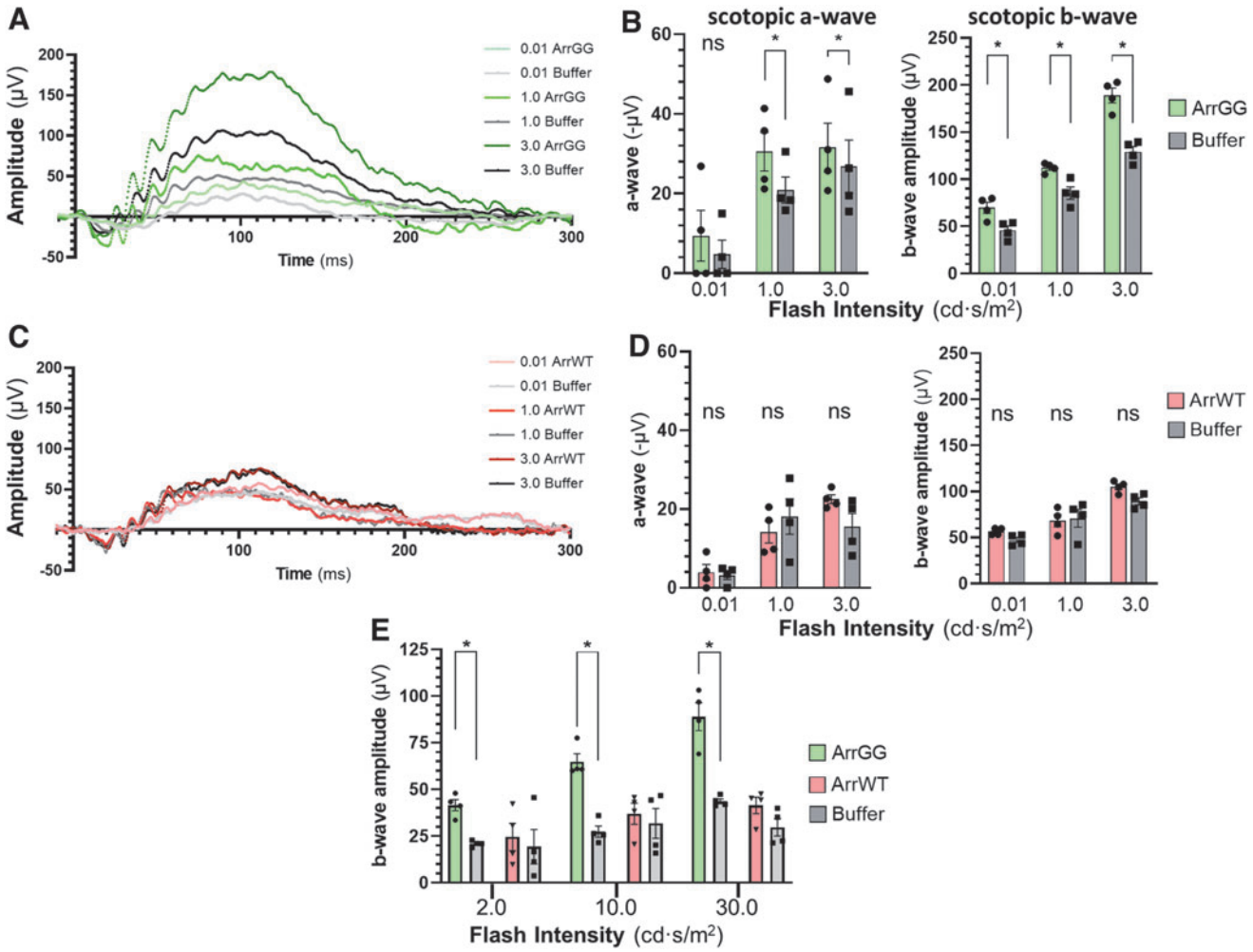


**Figure 4.** ERG responses in *P23H*$^{+/-}$ mice 100 days after injection with AAV-ArrGG or AAV-ArrWT. Mice were injected intravitreally with AAV in one eye, with the contralateral eye receiving buffer. **(A)** Example of scotopic ERG waveforms elicited in response to increasing intensities of light flashes for a *P23H*$^{+/-}$ mouse eye treated with ArrGG (*green traces*) compared with the contralateral eye injected with buffer (*gray traces*). **(B)** Summary quantitation of scotopic ERG response amplitudes at three flash intensities of a cohort of *P23H*$^{+/-}$ mice treated with ArrGG (*green bars*, $n=4$) or buffer (*gray bars*, $n=4$). **(C)** Example scotopic ERG response to increasing intensities of light flashes for a *P23H*$^{+/-}$ mouse eye treated with ArrWT (*red traces*) compared with the contralateral eye injected with buffer (*gray traces*). **(D)** Summary quantitation of scotopic ERG response amplitudes at three flash intensities of a cohort of *P23H*$^{+/-}$ mice treated with ArrWT (*red bars*, $n=4$) or buffer (*gray bars*, $n=4$). Bars represent mean ± SEM, with statistical significance of parametric paired *t*-test comparisons indicated with an *asterisk* ($\rho < 0.05$); ns, not significant. Average scotopic ERG amplitudes in a nondegenerating retina are –50 $\mu$V (0.01 cd), –140 $\mu$V (1.0 cd), and –150 $\mu$V (3.0 cd) for the a-wave and 200 $\mu$V (0.01 cd), 300 $\mu$V (1.0 cd), and 350 $\mu$V (3.0 cd) for the b-wave. **(E)** Summary quantitation of photopic ERG response amplitudes at three flash intensities of a cohort of *P23H*$^{+/-}$ mice treated with ArrGG in one eye (*green bars*, $n=4$) and buffer in the contralateral eye (*gray bars*, $n=4$), or treated with ArrWT in one eye (*red bars*, $n=4$) and buffer in the contralateral eye (*gray bars*, $n=4$). Bars indicate mean ± SEM, with statistical significance of parametric paired *t*-tests indicated with an *asterisk* ($\rho < 0.05$). Average photopic ERG amplitudes in a nondegenerating retina are 40 $\mu$V (2.0 cd), 60 $\mu$V (10.0 cd), and 80 $\mu$V (30.0 cd) for the b-wave. Color images are available online.

This conclusion is supported by two lines of evidence. First, our analysis of lactate production in retinas from the arrestin1 knockout mouse show that retinas with either reduced arrestin1 in *Arr1*$^{+/-}$ heterozygous mice or with completely absent arrestin1 (in *Arr1*$^{-/-}$) display elevated production of lactate. Second, we show that overexpression of the modified ArrGG, which functionally disinhibits enolase1 activity, results in increased lactate production. These two observations suggest a direct influence of arrestin1 on glycolytic output through enolase1 inhibition.

This *in vivo* increase of glycolysis through manipulation of arrestin1 interaction with enolase1 is somewhat surprising since enolase is generally not thought to be a rate-limiting enzyme in the glycolytic cascade. Instead, the rate of glycolysis is typically considered to be under allosteric control of phosphofructokinase.[42–44] However, two observations suggest a direct effect on glycolysis through enolase1. First, in our previous study using HEK-293T cells (which do not normally express arrestin1), it is only the addition of wild-type arrestin1 that causes a reduction in lactate production; addition of ArrGG causes

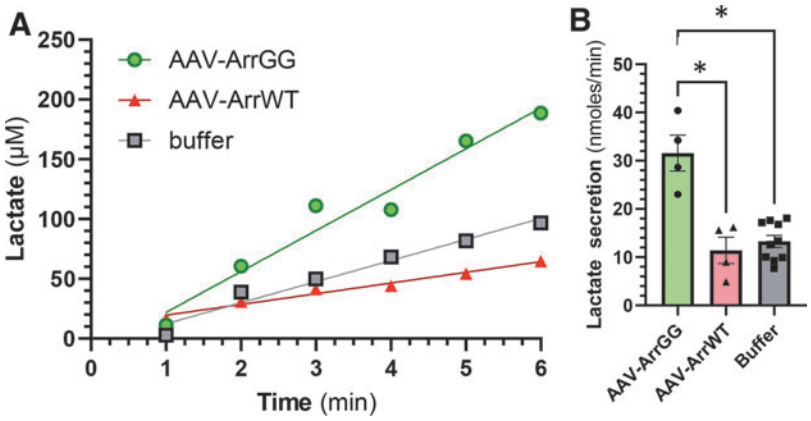


**Figure 5.** Rate of lactate secretion in excised *P23H*$^{+/-}$ retinas. Retinas were extracted 60 days postinjection and secreted lactate concentrations determined as described. **(A)** Examples of lactate secretion curves from retinas obtained from *P23H*$^{+/-}$ eyes treated with AAV-ArrGG (*green*), AAV-ArrWT (*red*), or buffer (*gray*). **(B)** Average lactate secretion rates in retinal explants from mice treated with ArrGG (*green*; $n=4$), with ArrWT (*red*; $n=4$), or buffer only (*gray*; $n=8$); bars show mean ± SEM, *asterisk* indicates statistically significant difference in one-way ANOVA with Tukey's *post hoc* comparison ($\rho < 0.05$). Color images are available online.

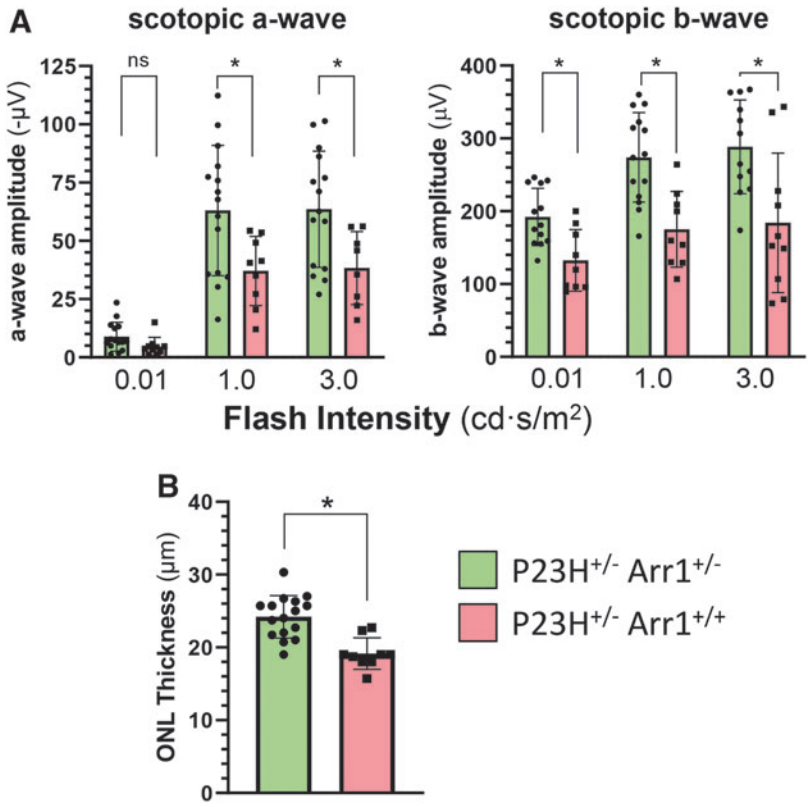


**Figure 6.** Photoreceptors are preserved in *P23H*$^{+/-}$ mice with reduced levels of Arr1 expression. **(A)** Summary quantitation of scotopic a-wave and b-wave ERG response amplitudes at three flash intensities of a cohort of *P23H*$^{+/-}$ mice (*red bars*, $n=9$; PN85 days) compared with *P23H*$^{+/-}$ mice in the background of *Arr1*$^{+/-}$ (*green bars*, $n=15$; PN100 days). Bars represent mean ± SD, with statistical significance of parametric, unpaired *t*-test comparisons indicated with an *asterisk* ($\rho < 0.05$); ns, not significant. **(B)** ONL thickness was measured in *P23H*$^{+/-}$ mice (*red bars*, $n=9$) from OCT images collected at PN92 days and in *P23H*$^{+/-}$ *Arr1*$^{+/-}$ mice at PN107 days (*green bars*, $n=16$); ONL measurements are shown at 1,200 μm from the optic nerve head in the temporal retina. Statistical comparison at each time point showed significantly thicker ONL in eyes of *P23H*$^{+/-}$ mice in the *Arr1*$^{+/-}$ background compared with eyes from *P23H*$^{+/-}$ mice in the *Arr1*$^{+/+}$ background (bars represent mean ± SD, with statistical significance of parametric, unpaired *t*-test comparisons indicated with an *asterisk* ($\rho < 0.05$). Color images are available online.

no change in lactate levels.[23] This observation argues against the idea that simply overexpressing any arrestin1 leads to some mechanism that suppresses lactate production.

Second, in the retina, enhanced lactate production is only measured when the ArrGG is overexpressed; overexpression of wild-type arrestin1 does not lead to increased lactate secretion. These opposite effects of the two forms of arrestin1 suggest the logical conclusion that the difference can be ascribed to the two amino acid changes present in ArrGG, which have been demonstrated to have a direct effect on enolase1 catalysis.

The possibility exists that the expression of the modified arrestin1 could have some other unknown consequence that leads to enhanced lactate production since arrestin1 is known to have a variety of interacting partners. These interactions include microtubules,[45–47] kinases (such as mitogen-activated protein kinase, extracellular-signal-related kinases 1 and 2, and c-Jun N-terminal kinase 3),[45,48,49] ubiquitin ligases,[45,49–51] and N-ethylmaleimide-sensitive factor.[52]

Furthermore, a recent study by Xue *et al.* shows that overexpression of one of the alpha-arrestins, thioredoxin-interacting protein, can lead to enhanced lactate catabolism.[16] Currently, nothing is known about the structure of arrestin1's complexes with these binding partners, such that it is impossible to predict whether the two glycine substitutions in ArrGG would have any impact on arrestin1's interaction with any of these other pathways.

However, our results showing that reducing arrestin1 expression (through heterozygous knockout of one *Arr1* allele) also slows photoreceptor loss in the *P23H*$^{+/-}$ mice offer strong evidence that the action of ArrGG is likely through direct effect on enolase1 rather than one of the other arrestin interaction partners. Nevertheless, additional studies are planned to more carefully measure glycolytic flux to precisely define mechanisms of the modified arrestin1's impact and investigate any potential role contributed through the other known arrestin1 interaction partners.

Regardless of the precise mechanism, it is clear that expression of ArrGG in the rhodopsin P23H heterozygous knock-in mouse model of retinitis pigmentosa has a protective effect that slows the rate of retinal degeneration. This protective effect is evidenced by both a morphologic preservation of photoreceptors and by a functional preservation of photoreceptor ERG response.

Interestingly, although we selectively targeted expression of ArrGG to rod photoreceptors specifically by using a human rod opsin promoter, we also demonstrated preservation of cone-driven ERG responses in ArrGG-treated eyes, suggesting a slowing of cone photoreceptor loss. Since the P23H-rhodopsin mutation is rod specific, the extension of cone survival likely reflects the well-established benefit cones receive through various mechanisms from delaying rod cell death, including rod-derived cone viability factor, structural support, and metabolic exchange.

In summary, our results show that although the application of ArrGG slows both the loss of photoreceptors and the decline of visual function compared with controls, there remains an age-related loss of photoreceptors. This continuing decline is not surprising since we are not targeting treatment of the underlying defect of the P23H rhodopsin mutation. Instead, we show that we can significantly alter the rate of photoreceptor loss. This slowing of vision loss can be a strongly positive outcome, particularly for IRDs where vision is not lost until the later decades of life.

We hypothesize that the modified arrestin1 might work in many examples of IRDs beyond those that involve mutations in the rhodopsin gene. Even though arrestin1 targets rhodopsin to quench phototransduction activation,[53] the therapeutic effect of ArrGG is mediated through its interaction with enolase1, involving the surface of arrestin1 that is not part of its interaction with rhodopsin.[23] Thus, this approach of using a modified arrestin1 to increase lactate production in photoreceptors offers a promising avenue for additional exploration for slowing vision loss in IRDs independent of the underlying genetic cause of the retinal degeneration. The idea of using this modified arrestin1 to slow vision loss in other models of inherited retinal degeneration beyond those caused by rhodopsin mutations will be a focus of future investigations.

## AUTHORS' CONTRIBUTIONS

All authors agree that they have participated in this work, contributing to the concept and design (T.S.N., F.D., A.D., and W.C.S.), analysis (T.N., C.S., and W.C.S.), and writing (T.S.N., F.D., C.S., A.D., and W.C.S.). The authors certify that this material has not been submitted or published in any other publication.

## ACKNOWLEDGMENTS

The authors are grateful for the expert help provided by Dr. Susan Bolch in conducting many of the animal experiments, and to Mr. Vince Chiodo and his team at the Ocular Gene Therapy Core for production of the AAV vectors used in this study.

## AUTHORS DISCLOSURE

W.C.S. and A.D. are inventors on a patent (PCT/US2021/022899) that describes the use of a modified arrestin1 for increasing lactate production in photoreceptors.

## FUNDING INFORMATION

This research was supported by funding from Foundation Fighting Blindness TA-NMT-0619-0770-UFL (WCS), the Oxnard Foundation, the National Institutes of Health grants EY026559 (AD) and S10OD028476 (WCS), and an unrestricted grant from Research to Prevent Blindness to the Department of Ophthalmology of University of Florida.

## REFERENCES


1. Berger W, Kloeckener-Gruissem B, Neidhardt J. The molecular basis of human retinal and vitreoretinal diseases. Prog Ret Eye Res 2010;29: 335–375.
2. Daiger SP, Bowne SJ, Sullivan LS. Perspective on genes and mutations causing retinitis pigmentosa. Arch Ophthalmol 2007;125:151–158.
3. Daiger SP, Sullivan LS, Bowne SJ. Genes and mutations causing retinitis pigmentosa. Clin Genet 2013;84:132–141.
4. Huang XF, Huang F, Wu KC, et al. Genotype-phenotype correlation and mutation spectrum in a large cohort of patients with inherited retinal dystrophy revealed by next-generation sequencing. Genet Med 2015;17:271–278.
5. Hauswirth WW, Aleman TS, Kaushal S, et al. Treatment of leber congenital amaurosis due to RPE65 mutations by ocular subretinal injection of adeno-associated virus gene vector: short-term results of a phase I trial. Hum Gene Ther 2008;19: 979–990.
6. Maguire AM, Simonelli F, Pierce EA, et al. Safety and efficacy of gene transfer for Leber's congenital amaurosis. N Engl J Med 2008;358:2240–2248.
7. Tuohy GP, Megaw R. A Systematic review and meta-analyses of interventional clinical trial studies for gene therapies for the inherited retinal degenerations (IRDs). Biomolecules 2021;11:760.
8. Yue L, Weiland JD, Roska B, et al. Retinal stimulation strategies to restore vision: fundamentals and systems. Prog Retin Eye Res 2016;53: 21–47.
9. Edwards TL, Cottriall CL, Xue K, et al. Assessment of the electronic retinal implant alpha AMS in restoring vision to blind patients with end-stage retinitis pigmentosa. Ophthalmology 2018;125: 432–443.
10. Simunovic MP, Shen W, Lin JY, et al. Optogenetic approaches to vision restoration. Exp Eye Res 2019;178:15–26.
11. Ahmed I, Johnston RJ, Jr., Singh MS. Pluripotent stem cell therapy for retinal diseases. Ann Transl Med 2021;9:1279.
12. Warburg O. On the origin of cancer cells. Science 1956;123:309–314.
13. Aït-Ali N, Fridlich R, Millet-Puel G, et al. Rod-Derived Cone Viability Factor promotes cone survival by stimulating aerobic glycolysis. Cell 2015; 161:817–832.
14. Xu L, Kong L, Wang J, et al. Stimulation of AMPK prevents degeneration of photoreceptors and the retinal pigment epithelium. Proc Natl Acad Sci U S A 2018;115:10475–10480.
15. Punzo C, Kornacker K, Cepko CL. Stimulation of the insulin/mTOR pathway delays cone death in a mouse model of retinitis pigmentosa. Nat Neurosci 2008;12:44.
16. Xue Y, Wang SK, Rana P, et al. AAV-Txnip prolongs cone survival and vision in mouse models of retinitis pigmentosa. eLife 2021;10:e66240.
17. Zhang L, Du J, Justus S, et al. Reprogramming metabolism by targeting sirtuin 6 attenuates retinal degeneration. J Clin Invest 2016;126:4659–4673.
18. Zhang L, Justus S, Xu Y, et al. Reprogramming towards anabolism impedes degeneration in a preclinical model of retinitis pigmentosa. Hum Mol Genet 2016;25:4244–4255.
19. Okawa H, Sampath AP, Laughlin SB, et al. ATP consumption by mammalian rod photoreceptors in darkness and in light. Curr Biol 2008;18:1917–1921.
20. Hurley JB, Lindsay KJ, Du J. Glucose, lactate, and shuttling of metabolites in vertebrate retinas. J Neurosci Res 2015;93:1079–1092.
21. Kanow MA, Giarmarco MM, Jankowski CSR, et al. Biochemical adaptations of the retina and retinal pigment epithelium support a metabolic ecosystem in the vertebrate eye. eLife 2017;6: e28899.
22. Smith WC, Bolch S, Dugger DR, et al. Interaction of arrestin with enolase1 in photoreceptors. Invest Ophthalmol Vis Sci 2011;52:1832–1840.
23. Miranda CJ, Fernandez N, Kamel N, et al. An arrestin-1 surface opposite of its interface with photoactivated rhodopsin engages with enolase-1. J Biol Chem 2020;295:6498–6508.
24. Chen J, Simon MI, Matthes MT, et al. Increased susceptibility to light damage in an arrestin knockout mouse model of Oguchi disease (Stationary night blindness). Invest Ophthalmol Vis Sci 1999;40:2978–2982.
25. Sakami S, Maeda T, Bereta G, et al. Probing mechanisms of photoreceptor degeneration in a new mouse model of the common form of autosomal dominant retinitis pigmentosa due to P23H opsin mutations. J Biol Chem 2011;286:10551–10567.
26. Laemmli UK. Cleavage of structural proteins during the assembly of the head of bacteriophage T4. Nature 1970;227:680–685.
27. Donoso L, Gregerson D, Smith L, et al. S-antigen: preparation and characterization of site-specific monoclonal antibodies. Curr Eye Res 1990;9:343–355.
28. Gibson DG, Young L, Chuang RY, et al. Enzymatic assembly of DNA molecules up to several hundred kilobases. Nat Methods 2009;6:343–345.
29. Lee J, Myers CA, Williams N, et al. Quantitative fine-tuning of photoreceptor cis-regulatory elements through affinity modulation of transcription factor binding sites. Gene Ther 2010;17:1390–1399.
30. Petrs-Silva H, Dinculescu A, Li Q, et al. Novel properties of tyrosine-mutant AAV2 vectors in the mouse retina. Mol Ther 2011;19:293–301.
31. Kay CN, Ryals RC, Aslanidi GV, et al. Targeting photoreceptors via intravitreal delivery using novel, capsid-mutated AAV vectors. PLoS One 2013;8:e62097.
32. Zolotukhin S, Potter M, Zolotukhin I, et al. Production and purification of serotype 1, 2, and 5 recombinant adeno-associated viral vectors. Methods 2002;28:158–167.
33. Chinchore Y, Begaj T, Wu D, et al. Glycolytic reliance promotes anabolism in photoreceptors. Elife 2017;6:e25946.
34. Rueda EM, Johnson JE, Giddabasappa A, et al. The cellular and compartmental profile of mouse retinal glycolysis, tricarboxylic acid cycle, oxidative phosphorylation, and ~P transferring kinases. Mol Vision 2016;22:847–885.
35. Sokolov M, Lyubarsky AL, Strissel KJ, et al. Massive light-driven translocation of transducin between the two major compartments of rod cells: a novel mechanism of light adaptation. Neuron 2002;34:95–106.
36. Jeon C-J, Strettoi E, Masland RH. The major cell populations of the mouse retina. J Neurosci 1998; 18:8936–8946.
37. Chiang W-C, Kroeger H, Sakami S, et al. Robust endoplasmic reticulum-associated degradation of rhodopsin precedes retinal degeneration. Mol Neurobiol 2015;52:679–695.
38. Comitato A, Di Salvo MT, Turchiano G, et al. Dominant and recessive mutations in rhodopsin activate different cell death pathways. Hum Mol Genet 2016;25:2801–2812.
39. Liu H, Tang J, Du Y, et al. Photoreceptor cells influence retinal vascular degeneration in mouse models of retinal degeneration and diabetes. Invest Ophthalmol Vis Sci 2016;57:4272–4281.
40. Mitra RN, Zheng M, Weiss ER, et al. Genomic form of rhodopsin DNA nanoparticles rescued autosomal dominant Retinitis pigmentosa in the P23H knock-in mouse model. Biomaterials 2018; 157:26–39.
41. Nakamura PA, Shimchuk AA, Tang S, et al. Small molecule Photoregulin3 prevents retinal degeneration in the RhoP23H mouse model of retinitis pigmentosa. eLife 2017;6:e30577.
42. Boscá L, Corredor C. Is phosphofructokinase the rate-limiting step of glycolysis? Trends Biochem Sci 1984;9:372–373.
43. Nelson DL, Cox MM, Lehninger AL. Lehninger Principles of Biochemistry, 7th ed. New York, NY: W.H. Freeman, 2017.
44. Shestov AA, Liu X, Ser Z, et al. Quantitative determinants of aerobic glycolysis identify flux through the enzyme GAPDH as a limiting step. eLife 2014;3:e03342.
45. Hanson SM, Cleghorn WM, Francis DJ, et al. Arrestin mobilizes signaling proteins to the cytoskeleton and redirects their activity. J Mol Biol 2007;368:375–387.

46. Hanson SM, Francis DJ, Vishnivetskiy SA, et al. Visual arrestin binding to microtubules involves a distinct conformational change. J Biol Chem 2006; 281:9765–9772.

47. Nair KS, Hanson SM, Kennedy MJ, et al. Direct binding of visual arrestin to microtubules determines the differential subcellular localization of its splice variants in rod photoreceptors. J Biol Chem 2004;279:41240–41248.

48. Song X, Coffa S, Fu H, et al. How does arrestin assemble MAPKs into a signaling complex? J Biol Chem 2009;284:685–695.

49. Song X, Gurevich EV, Gurevich VV. Cone arrestin binding to JNK3 and Mdm2: conformational preference and localization of interaction sites. J Neurochem 2007;103:1053–1062.

50. Ahmed MR, Zhan X, Song X, et al. Ubiquitin ligase parkin promotes Mdm2-arrestin interaction but inhibits arrestin ubiquitination. Biochemistry 2011; 50:3749–3763.

51. Song X, Raman D, Gurevich EV, et al. Visual and both non-visual arrestins in their "inactive" conformation bind JNK3 and Mdm2 and relocalize them from the nucleus to the cytoplasm. J Biol Chem 2006;281:21491–21499.

52. Huang S-P, Brown BM, Craft CM. Visual arrestin 1 acts as a modulator for N-ethylmaleimide-sensitive factor in the photoreceptor synapse. J Neurosci 2010;30:9381–9391.

53. Wilden U, Hall SW, Kühn H. Phosphodiesterase activation by photoexcited rhodopsin is quenched when rhodopsin is phosphorylated and binds the intrinsic 48-kDa protein of rod outer segments. Proc Natl Acad Sci U S A 1986;83:1174–1178.

Received for publication November 5, 2021; accepted after revision January 23, 2022.

Published online: January 26, 2022.